



## A non-autonomous mega-extreme multistable chaotic system

Atefeh Ahmadi<sup>a</sup>, Sriram Parthasarathy<sup>b</sup>, Hayder Natiq<sup>c,d</sup>, Sajad Jafari<sup>a,e</sup>, Igor Franović<sup>f,\*</sup>, Karthikeyan Rajagopal<sup>g</sup>

<sup>a</sup> Department of Biomedical Engineering, Amirkabir University of Technology (Tehran Polytechnic), Tehran, Iran

<sup>b</sup> Centre for Computational Modelling, Chennai Institute of Technology, Chennai 600069, Tamil Nadu, India

<sup>c</sup> Ministry of Higher Education and Scientific Research, Baghdad 10024, Iraq

<sup>d</sup> Department of Computer Technology Engineering, College of Information Technology, Imam Ja'afar Al-Sadiq University, Baghdad 10001, Iraq

<sup>e</sup> Health Technology Research Institute, Amirkabir University of Technology (Tehran Polytechnic), Tehran, Iran

<sup>f</sup> Scientific Computing Laboratory, Center for the Study of Complex Systems, Institute of Physics Belgrade, University of Belgrade, Pregrevica 118, 11080 Belgrade, Serbia

<sup>g</sup> Centre for Nonlinear Systems, Chennai Institute of Technology, Chennai 600069, Tamil Nadu, India

### ARTICLE INFO

#### Keywords:

Megastability

Extreme multistability

Coexisting attractors

Connecting curves

Analog circuit design

### ABSTRACT

Megastable and extreme multistable systems comprise two major new branches of multistable systems. So far, they have been studied separately in various chaotic systems. Nevertheless, to the best of our knowledge, no chaotic system has so far been reported that possesses both types of multistability. This paper introduces the first three-dimensional non-autonomous chaotic system that displays megastability and extreme multistability, jointly called mega-extreme multistability. Our model shows extreme multistability for a variation of an initial condition associated with one system variable and megastability concerning another variable. The different types of coexisting attractors are characterized by the corresponding phase portraits and first return maps, as well as by constructing the appropriate bifurcation diagrams, calculating the Lyapunov spectra, the Kaplan-Yorke dimension and the connecting curves, and by determining the corresponding basins of attraction. The system is explicitly shown to be dissipative, with the dissipation being state-dependent. We demonstrate the feasibility and applicability of our model by designing and simulating an appropriate analog circuit.

### 1. Introduction

The foundation stone of chaos theory was laid by Edward Lorenz in 1963, having introduced a simplified model of atmospheric convection whose evolution, surprisingly at that point, turned out to sensitively depend on initial conditions [1]. Since then, concepts from chaos theory have permeated almost every branch of science and engineering, triggering profound changes of paradigm in physics, chemistry, climate and environmental sciences, optics, electronics, pharmacology, medicine, economy, and sociology, to name but a few [2]. Chaos theory describes complex nonlinear systems such as the earth's atmosphere, animal populations, lasers, fluid flows, pathological heartbeat and brain activity patterns, and geological processes [3–5], whose long-term dynamics are intrinsically unpredictable despite their deterministic nature [6,7]. The global stability of dynamics on a chaotic attractor counteracts the local instability in the sense that statistical (average) properties can be predictable even if the detailed dynamics are not [7].

Another type of nonlinear systems whose dynamics critically

depends on initial conditions are multistable systems [8–10], which possess multiple coexisting attractors for a given set of parameters. Examples of multistable behavior have been found in various fields, from biology, ecology, climatology, and neuroscience to laser and semiconductor physics, chemical reactions, and social systems [11–13]. Multistability emerges generically in several classes of systems, including weakly dissipative systems, coupled systems and systems with time-delayed feedback and/or interactions [8–10]. The problems of constructing multistable systems with desired properties and controlling the switching dynamics between the coexisting states have catalyzed intense research in theory and applications [9]. Specific methods have been developed to discover and generate coexisting attractors in dynamical systems, like amplitude control [14], offset boosting [15,16], and offset parameter cancellation [17]. While multistability has classically been associated with the coexistence of a finite number of attractors, within the last decade, it has come to light that there is indeed an entirely new realm of dissipative systems that feature infinitely many coexisting attractors [18–21]. Moreover, two distinct classes of such

\* Corresponding author.

E-mail address: [franovic@ipb.ac.rs](mailto:franovic@ipb.ac.rs) (I. Franović).

systems have been discovered: on the one hand, systems with *extreme multistability* [22–28] possess *uncountable* infinitely many attractors, such that a continuous variation of initial conditions may induce bifurcations [29–31]; at the other hand, *megastable systems* [32–34] exhibit *countable* many nested coexisting attractors, and the corresponding initial conditions cannot act as additional bifurcation parameters [35–37].

In the present paper, we introduce the first system exhibiting mega and extreme multistability features. The model comprises a non-autonomous three-dimensional system that can present chaotic, torus, and periodic attractors. We show how the mega and extreme multistability features manifest themselves with respect to the variation of initial conditions corresponding to two different state variables. To the best of our knowledge, such a system has previously not been reported in the literature.

The paper is organized as follows. Section 2 introduces our model of a non-autonomous chaotic system and studies its dynamical regimes by providing the relevant phase portraits and first return maps. Also, the dissipative character of system dynamics is explicitly demonstrated, and the connecting curves are calculated to illustrate the underlying attractors' structure better. Section 3 addresses the extreme multistability feature of the system dynamics, involving the appropriate bifurcation diagrams, calculation of the Lyapunov exponents spectra and Kaplan-Yorke dimension, and an analysis of the basins of attraction. The applicability of the proposed model is demonstrated by analog circuit simulations in Section 4. Section 5 provides a summary of our main results.

## 2. The non-autonomous chaotic system

The model we introduce is a three-dimensional non-autonomous system given by

$$\begin{cases} \dot{x} = y \\ \dot{y} = z + y\cos(x) \\ \dot{z} = -by + A\omega\cos(\omega t) \end{cases}, \quad (1)$$

where  $A\omega\cos(\omega t)$  is the forcing term with an amplitude  $A$  and frequency  $\omega$ , while  $b$  is another control parameter.

Having fixed the forcing and intrinsic system parameters to  $A = 0.8$ ,  $b = 0.1$ ,  $\omega = 0.7$ , we observe three different types of attractors of System (1) under variation of initial conditions, see Fig. 1. In the top row are shown the phase portrait projections in the  $Y - Z$  plane, whereas in the bottom row are provided the corresponding first return maps obtained by collecting the successive maxima of the  $Y$  signal. The initial conditions are given by  $(x_0, y_0, z_0) = (0, 0, z_0)$  whereby  $z_0$  is respectively set to zero,  $-0.3$ , and  $2.2$  in the left, middle, and right columns of Fig. 1. It turns out that System (1) can exhibit three different types of dynamics by varying the initial condition  $z_0$ . In particular, the solutions in Fig. 1(a)–(c) display chaotic, periodic (period 3), and torus attractors, respectively. The number of points in Fig. 1(e) corresponds to the period of the attractor in Fig. 1(b). The general pattern of the return maps in Fig. 1(d) and (f) are similar, although the one for the torus attractor in Fig. 1(f) shows a more ordered structure. The areas of phase space occupied by the chaotic and torus attractors are approximately the same, but the sequences of points in the return maps are entirely different.

Fig. 1 demonstrates that the continuous variation of the initial condition  $z_0$  can indeed give rise to bifurcations, which is a signature of the extreme multistability of System (1).

To show the megastability of this system, two different values of  $z_0$  are chosen, and the megastability feature under varying  $y_0$  is demonstrated separately for each of the two given  $z_0$  values. The phase portraits of System (1) with  $A = 0.8$ ,  $b = 0.1$ ,  $\omega = 0.7$  and initial conditions  $x_0 = 0, y_0 \in \{0, 5, 7\}, z_0 \in \{0, -0.9\}$  are shown in Fig. 2(a) and (b),  $z_0$  is set to zero and  $-0.9$ , respectively. In both panels, the blue, orange, and yellow attractors correspond to  $y_0 = 0, y_0 = 5$ , and  $y_0 = 7$ , respectively. All coexisting attractors are chaotic in Fig. 2(a), whereas in Fig. 2(b), two are periodic, and the outermost one is chaotic. It should be noted that only three of the coexisting attractors are plotted in this figure, and changing  $y_0$  leads to an infinite but countable number of coexisting attractors, which conforms to the megastability property. On the other hand, variation of  $z_0$  gives rise to an infinite and uncountable

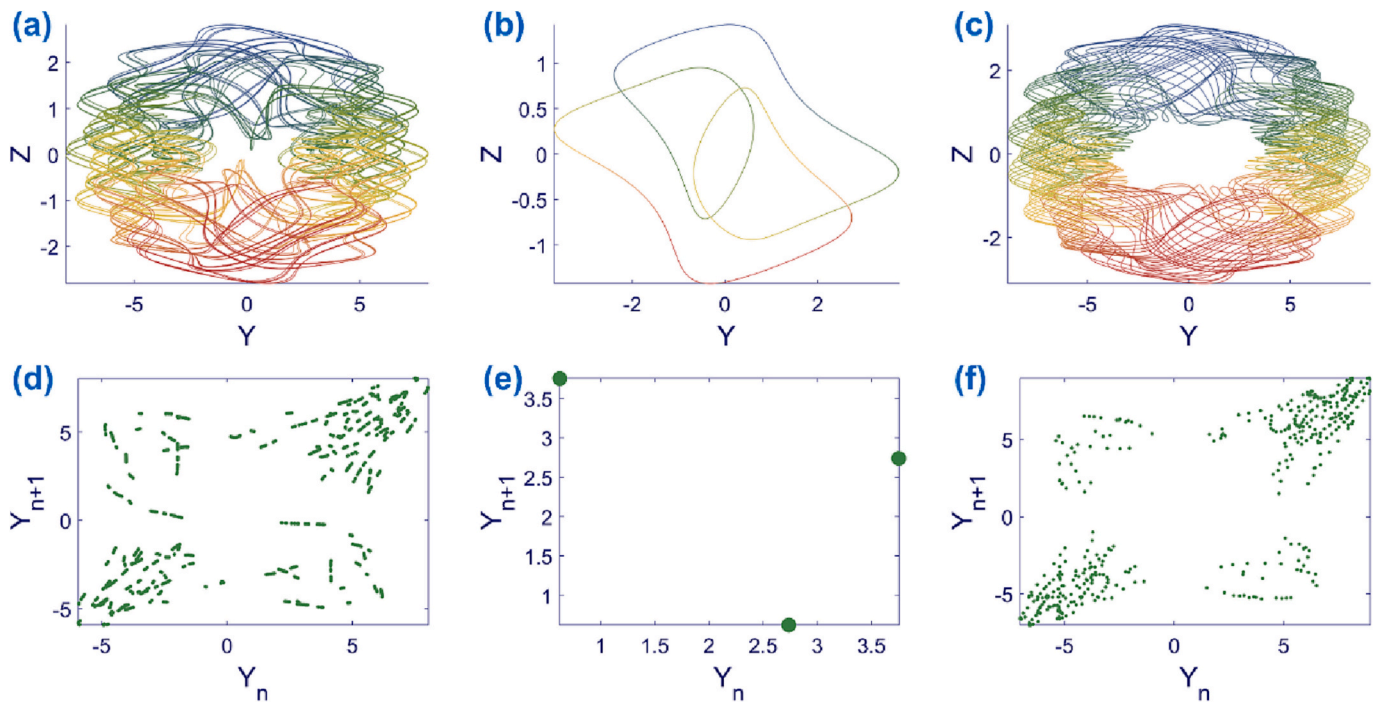
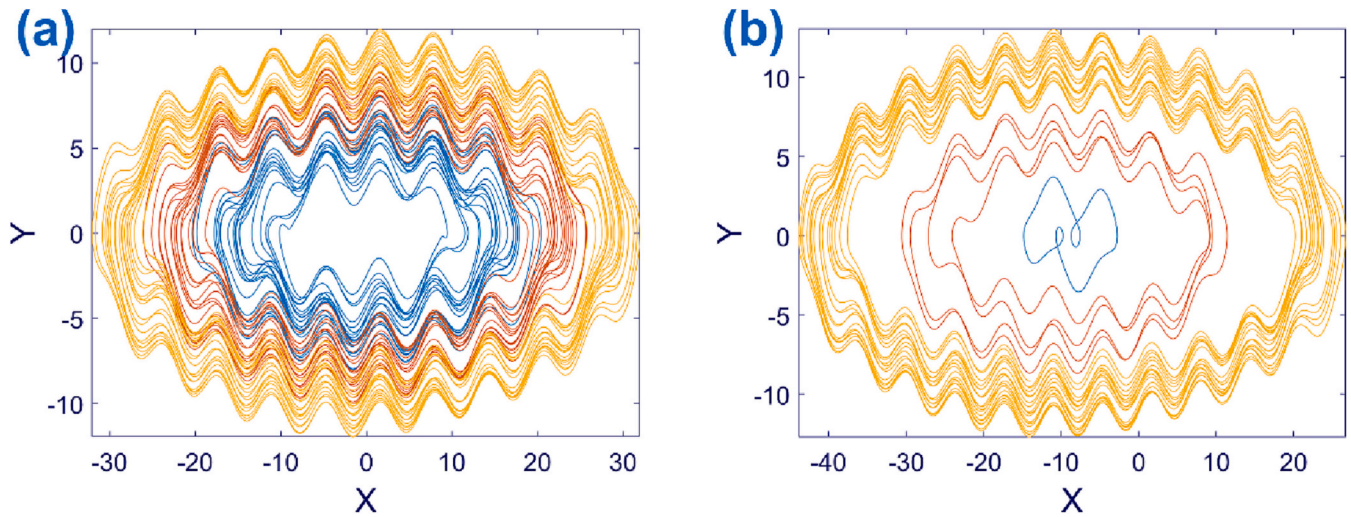


Fig. 1. Phase portrait projections in the  $Y - Z$  plane and return maps of System (1) for fixed  $A = 0.8, b = 0.1, \omega = 0.7$  and initial conditions  $(x_0, y_0, z_0) = (0, 0, z_0)$ . By changing  $z_0$ , three different types of behaviors are observed. (a) and (d): chaotic dynamics with  $z_0 = 0$ , (b) and (e): periodic dynamics with  $z_0 = -0.3$ , and (c) and (f): torus-like dynamic with  $z_0 = 2.2$ . The corresponding first return maps are constructed by collecting the maximum values of the  $Y$  signal.



**Fig. 2.** Phase portrait projections in the  $X - Y$  plane of **System (1)** with fixed  $A = 0.8, b = 0.1, \omega = 0.7$  and initial conditions  $(x_0, y_0, z_0) = (0, y_0, z_0)$  where  $y_0 \in \{0, 5, 7\}$ . **(a)** Coexisting chaotic attractors with  $z_0 = 0$  and **(b)** coexisting periodic and chaotic attractors for  $z_0 = -0.9$ . Blue, orange, and yellow attractors correspond to  $y_0 = 0, y_0 = 5$ , and  $y_0 = 7$ , respectively. For each given value of  $z_0$ , **System (1)** exhibits an infinite but countable number of coexisting attractors under the variation of  $y_0$ , which confirms its megastability. (For interpretation of the references to color in this figure legend, the reader is referred to the web version of this article.)

number of coexisting attractors, a hallmark of extreme multistability. In summary, **System (1)** shows extreme multistability concerning the variation of  $z_0$ , but for any arbitrary value of  $z_0$ , it is megastable under the variation of  $y_0$ . Therefore, **System (1)** can be called a mega-extreme multistable system.

### 2.1. Dissipative character of system dynamics

The energy dissipation of a dynamical system is calculated by the trace of the system's Jacobian matrix, which is equal to the divergence of the system. The Jacobian matrix and divergence of **System (1)** are calculated as

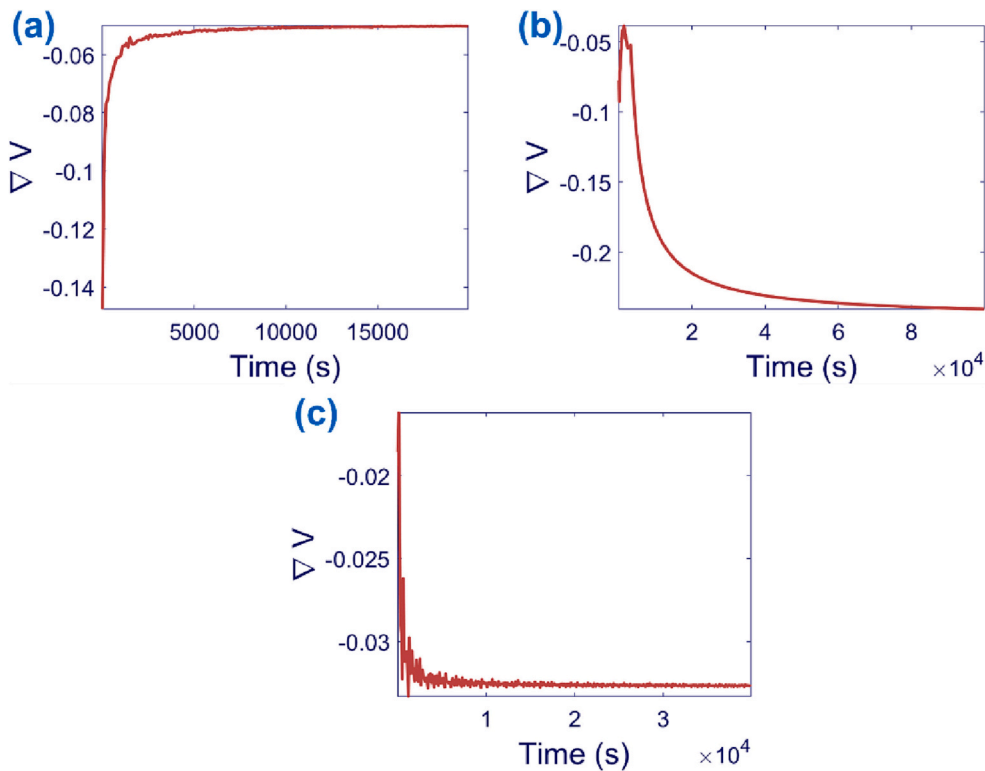


**Fig. 3.** The average divergence for **System (1)** with  $A = 0.8, b = 0.1, \omega = 0.7$  and initial conditions  $(x_0, y_0, z_0) = (0, 0, z_0)$ : **(a)**  $z_0 = 0$  (chaotic behavior), **(b)**  $z_0 = -0.3$  (periodic behavior), and **(c)**  $z_0 = 2.2$  (quasiperiodic dynamics). Note that all three average divergences converge to a negative value, indicating that all three types of dynamics are indeed system attractors.

$$J = \begin{bmatrix} 0 & 1 & 0 \\ -y\sin(x) & \cos(x) & 1 \\ 0 & -b & 0 \end{bmatrix} \rightarrow \nabla V = \text{Tr}(J) = \cos(x) \quad (2)$$

Eq. (2) implies that the energy dissipation depends on the value of the  $x$  state variable. For such a scenario, one should calculate the average value of the divergence  $\nabla V$ , whereby the negative, zero, and positive values conform to dissipative, conservative, and explosive dynamics, respectively. The divergence is calculated for each system attractor separately and does not determine the overall system's behavior.

The average value of divergence for System (1) with  $A = 0.8, b = 0.1, \omega = 0.7$  and initial conditions  $(x_0, y_0, z_0) = (0, 0, z_0)$  is plotted in Fig. 3. The value of  $z_0$  is set to zero,  $-0.3$ , and  $2.2$  in panels (a)–(c). The runtimes in each simulation are adapted to ensure the convergence of the average dissipation. Note that Fig. 3 corroborates that for each of the three previously discussed examples of system dynamics, one finds a negative average divergence, implying the existence of genuine attractors.

### 2.2. Connecting curves

While the equilibrium points of a dynamical system can help determine the position of attractors locally, the connecting curves can provide information on a more global landscape [38]. In particular, the connecting curves highlight the direction in which the attractor swirls [39]. While the fixed points are classically called zero-dimensional invariant sets, the connecting curves are nevertheless one-dimensional invariant sets [40]. Consider the flow  $\vec{S} = (x(t), y(t), z(t))^T$  that includes all three state variables. The velocity field  $\vec{V}(t)$  is then given by  $\frac{d\vec{S}}{dt} = \vec{V}(t) = (f_1, f_2, f_3)$  where  $f_1, f_2, f_3$  are the right-hand side expressions in a set of ordinary differential equations. The acceleration field  $\vec{A}(t)$  is calculated as

$$\frac{d\vec{V}}{dt} = \vec{A}(t) = \frac{\partial \vec{V}}{\partial \vec{S}} \frac{d\vec{S}}{dt} \rightarrow \vec{A}(t) = J\vec{V}(t) = \lambda\vec{V}(t) \rightarrow J\vec{V}(t) - \lambda\vec{V}(t) = 0 \quad (3)$$

Applying the chain rule in Eq. (3), the acceleration field is shown to be proportional to the velocity field. Finally, the connecting curves satisfy the condition  $J\vec{V}(t) - \lambda\vec{V}(t) = 0$  [41].

System (3) leads to an equation for each state variable. Nevertheless, the number of unknowns is four (three state variables and  $\lambda$ ). To solve these equations, a state variable must be selected as the principal state variable: in our case, variable  $y$  is selected. Afterward, all other state variables (here  $x$  and  $z$ ) and  $\lambda$  should be written in terms of the principal state variable. The principal state variable should be chosen to simplify the calculations. Next, considering the attractor's position in space, a desired interval is selected for the state variable  $y$ , and for each point in that interval, the value of  $\lambda$  and other state variables are calculated. In the case of System (1),  $\lambda$  is independent of  $y$  and is always zero. Consequently,  $x$  and  $z$  only depend on  $y$ , so there can be four different

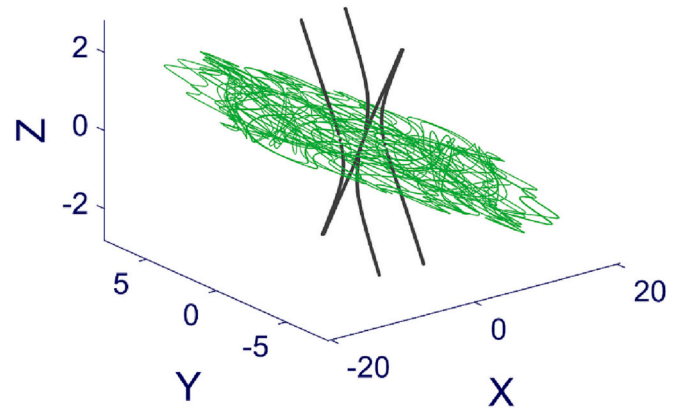


Fig. 4. Chaotic attractor and connecting curves of System (1) with  $A = 0.8, b = 0.1, \omega = 0.7$  and initial conditions  $(x_0, y_0, z_0) = (0, 0, 0)$ . The black lines are the connecting curves showing the direction around which the attractor swirls. Four black lines correspond to four pairs of  $x$  and  $z$  in Table 1.

solutions for different combinations of  $x$  and  $z$ , see Table 1. The corresponding connecting curves of System (1) with its chaotic attractor are depicted in Fig. 4. The system parameters are  $A = 0.8, b = 0.1, \omega = 0.7$  and the initial conditions are  $(x_0, y_0, z_0) = (0, 0, 0)$ . The connecting curves (black lines) provide global information about the attractor position and curvature.

### 3. Extreme multistability

To study the extreme multistability of System (1), we consider its initial conditions-dependent dynamics via the bifurcation diagram, Lyapunov exponents, Kaplan-Yorke dimension and attraction basins. The bifurcation diagram and the corresponding Kaplan-Yorke dimension of System (1) are shown in Fig. 5 using the initial condition  $z_0$  as a control parameter that varies within the interval  $[-3, 3]$ . The system parameters are set to  $A = 0.8, b = 0.1, \omega = 0.7$ , whereas the remaining initial conditions are fixed to  $(x_0, y_0) = (0, 0)$ . The bifurcation diagram in Fig. 5(a) is constructed by plotting the local maxima of the  $Z$  state variable. One observes that System (1) continuously switches between the periodic and chaotic behaviors within the selected  $z_0$  interval. The Kaplan-Yorke dimension  $D_{KY}$  shown in Fig. 5(b) is defined as [42,43]

$$D_{KY} = j + \frac{\sum_{i=1}^j \lambda_i}{|\lambda_{j+1}|}, \sum_{i=1}^j \lambda_i \geq 0, \sum_{i=1}^{j+1} \lambda_i < 0, \quad (4)$$

where  $\lambda_i$  are Lyapunov exponents. Note that in order to calculate  $D_{KY}$ , all Lyapunov exponents should be sorted in descending order, whereby  $j$  in Eq. (4) denotes the index of the Lyapunov exponent up to which the sum of Lyapunov exponents is non-negative. The latter implies that the  $D_{KY}$  of chaotic, torus, and periodic attractors are larger than two, equal to

Table 1

$x$  and  $z$  state variables in terms of  $y$  for solving Eq. (3). The value of  $\lambda$  is not related to  $y$  and is always zero.  $y$  state variable is treated as the principal state variable to simplify the mathematical operations. Four different pairs of  $x$  and  $z$  can be considered in calculating the connecting curves.

$\lambda$	$x$	$z$
0	$2 \tan^{-1} \left( \frac{\sqrt{(5y-4)(10y+7)(50y^2+5y+28)} - 50y^2}{5y+28} \right)$	$-\frac{\sqrt{(5y-4)(10y+7)(50y^2+5y+28)}}{50y}$
0	$-2 \tan^{-1} \left( \frac{\sqrt{(5y-4)(10y+7)(50y^2+5y+28)} + 50y^2}{5y+28} \right)$	$\frac{\sqrt{(5y-4)(10y+7)(50y^2+5y+28)}}{50y}$
0	$2 \tan^{-1} \left( \frac{\sqrt{(5y+4)(10y-7)(50y^2-5y+28)} - 50y^2}{5y-28} \right)$	$-\frac{\sqrt{(5y+4)(10y-7)(50y^2-5y+28)}}{50y}$
0	$-2 \tan^{-1} \left( \frac{\sqrt{(5y+4)(10y-7)(50y^2-5y+28)} + 50y^2}{5y-28} \right)$	$\frac{\sqrt{(5y+4)(10y-7)(50y^2-5y+28)}}{50y}$

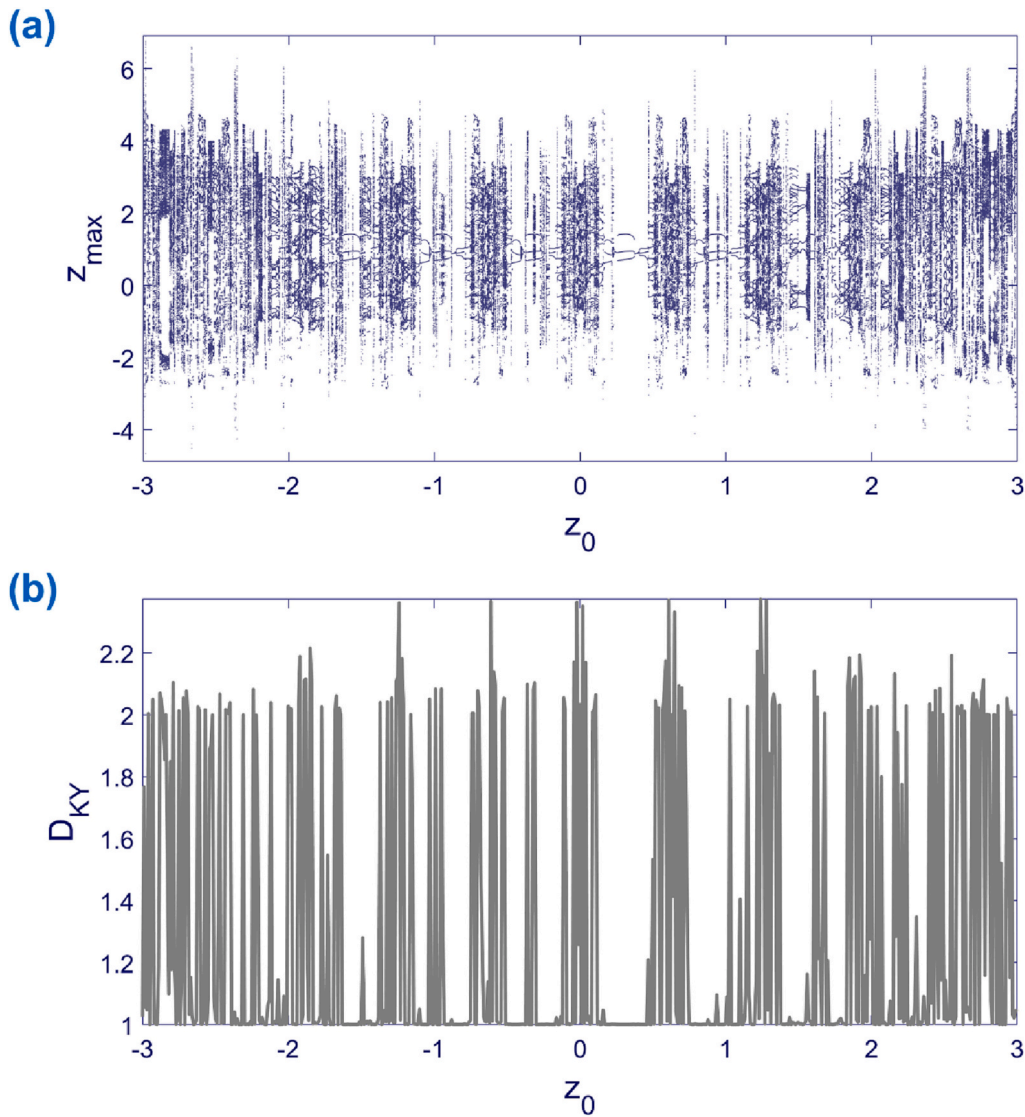


**Fig. 5.** Bifurcation diagram and  $D_{KY}$  of **System (1)** with  $A = 0.8, b = 0.1, \omega = 0.7$  for fixed initial conditions  $(x_0, y_0) = (0, 0)$  while varying  $z_0$  in the  $[-3, 3]$  interval. **(a)** Bifurcation diagram showing the local maxima of  $Z$  state variable and **(b)** the corresponding  $D_{KY}$ . **System (1)** exhibits chaotic or periodic attractors in the selected interval.  $D_{KY}$  matches the bifurcation diagram because its value is more than two in chaotic regions and one within periodic windows.

two, and equal to one, respectively. The variation of  $D_{KY}$  in **Fig. 5(b)** is indeed consistent with the bifurcation diagram from **Fig. 5(a)**.

The Lyapunov exponents of **System (1)** with the same parameters as in **Fig. 5(a)** and  $z_0$  as the control parameter are provided in **Fig. 6**. **Fig. 6(a)** shows the variation of the first two *largest* Lyapunov exponents with  $z_0$ , while **Fig. 6(b)** indicates the changes of the *smallest* one. The smallest Lyapunov exponent is always zero, but the exponents can have different values according to the system's dynamics. For chaotic attractors of a three-dimensional system, the Lyapunov spectrum contains one positive, one negative, and one zero exponent, whereby the value of the positive exponent is less than the absolute value of the negative one. On the other hand, the Lyapunov spectrum of a periodic attractor contains one zero and two negative exponents. Finally, one observes one negative and two zero exponents for torus attractors. The changes between the system attractors with  $z_0$  reflected in the Lyapunov spectra from **Fig. 6** are consistent with the results from **Fig. 5**.

Another important tool to investigate the multistable systems is to identify the corresponding attraction basins. **Fig. 7** shows the attraction basins for the dynamics of **System (1)** with  $A = 0.8, b = 0.1, \omega = 0.7$ , obtained by fixing one initial condition to zero and varying the other two. The attraction basins are plotted in (a)  $x_0 - y_0$  plane with  $x_0 \in [2, 5]$

and  $y_0 \in [-4, 2]$ , (b)  $x_0 - z_0$  plane with  $x_0 \in [-3, 3], z_0 \in [-1, 1]$ , and (c)  $y_0 - z_0$  plane with  $y_0 \in [-4, 4]$  and  $z_0 \in [-1, 1]$ . The intervals of initial conditions are chosen to avoid the torus attractors. Yellow and blue-green colors represent chaotic and periodic solutions, respectively. For periodic solutions, the representing color encodes the period. In **Fig. 7(b)** and (c), where the initial condition  $z_0$  is varied, one may observe the same transitions between the different periodic and chaotic attractors, as illustrated in the bifurcation diagram in **Fig. 5(a)**.

#### 4. Analog circuit design

To corroborate the previous numerical simulations, we have designed an analog circuit of **System (1)** given by

$$\begin{cases} \dot{X} = \frac{1}{R_1 C_1} Y \\ \dot{Y} = \frac{1}{R_2 C_2} Z + \frac{1}{R_3 C_2} Y \cos(X) \\ \dot{Z} = -\frac{1}{R_4 C_3} Y + \frac{1}{R_5 C_3} \cos(0.7t) \end{cases} \quad (5)$$

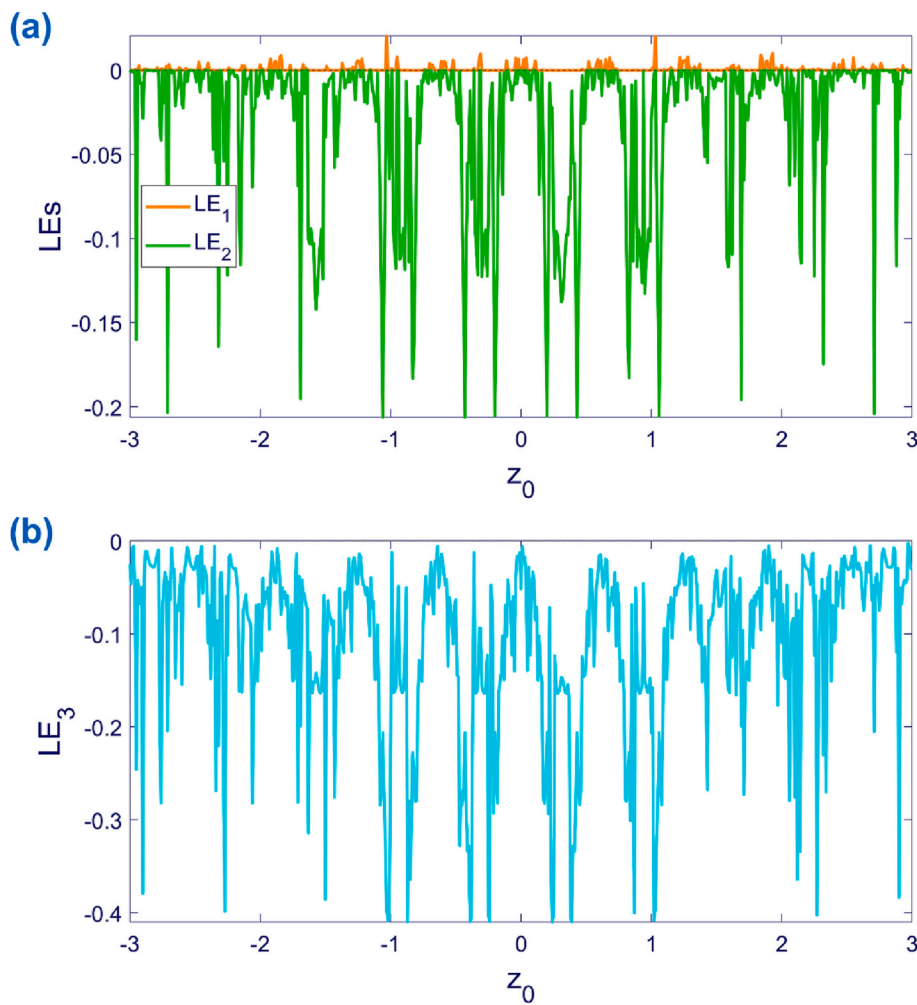


**Fig. 6.** Lyapunov exponents of **System (1)** with  $A = 0.8, b = 0.1, \omega = 0.7$  and for fixed initial conditions  $(x_0, y_0) = (0, 0)$  under variation of  $z_0$  within the  $[-3, 3]$  interval. **(a)** Two largest Lyapunov exponents and **(b)** the smallest Lyapunov exponent. While the smallest Lyapunov exponent is always zero, the other two exponents in **(a)** can have different values. If the latter are one positive and one zero (the positive exponent is less than the absolute value of the negative one), the attractor is chaotic. The attractor is periodic with one zero and one negative exponent in **(a)**. The Lyapunov exponents corroborate the type of solutions from the bifurcation diagram in **Fig. 5**.

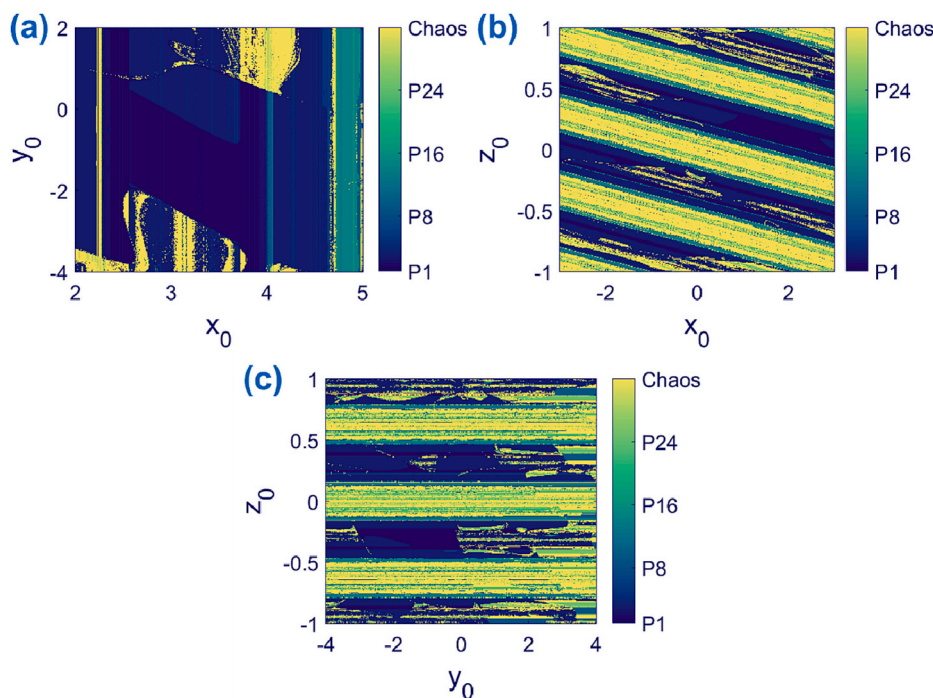


**Fig. 7.** Attraction basins of **System (1)** with  $A = 0.8, b = 0.1, \omega = 0.7$ . **(a)** On  $x_0 - y_0$  plane with  $x_0 \in [2, 5], y_0 \in [-4, 2]$ , and  $z_0 = 0$ , **(b)** on  $x_0 - z_0$  plane with  $x_0 \in [-3, 3], z_0 \in [-1, 1]$ , and  $y_0 = 0$  and, and **(c)** on  $y_0 - z_0$  plane with  $y_0 \in [-4, 4], z_0 \in [-1, 1]$ , and  $x_0 = 0$ . A  $300 \times 300$  grid of initial conditions is used to obtain each basin of attraction. Yellow and blue-green colors represent the chaotic and periodic solutions, respectively. As the period of the periodic attractor increases, its representative color changes from blue to green. The transitions between the different types of attractors from **Fig. 5** **(a)** are recovered in **(b)** and **(c)**, where one of the variable initial conditions is  $z_0$ .

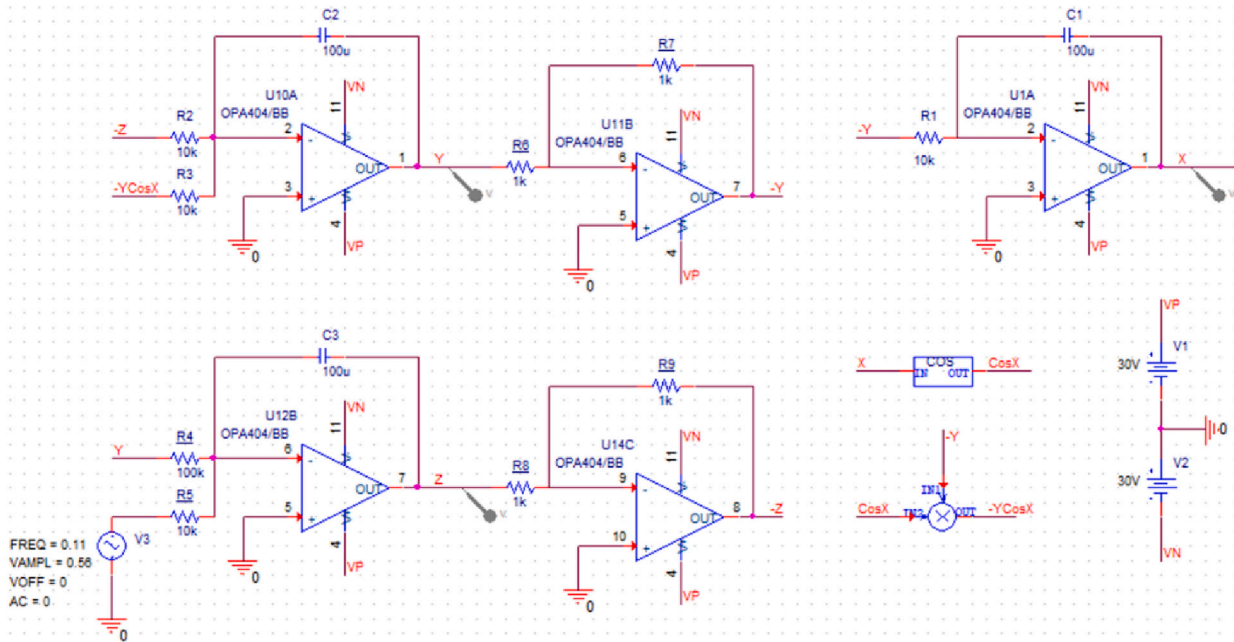


**Fig. 8.** The analog circuit following System (5) is implemented in OrCAD. The particular circuit elements are  $C_1 = C_2 = C_3 = 100\mu F$  and  $R_1 = R_2 = R_3 = R_5 = 10k\Omega, R_4 = 100k\Omega, R_6 = R_7 = R_8 = R_9 = 1k\Omega$ . The supply voltages of the OpAmps are set to  $V_p = 30V, V_n = -30V$ . Three integrator and two inverter circuits are implemented based on OpAmps. Also, one multiplier, one cosine function block, and one cosine (sine with a  $\frac{\pi}{2}$ rad phase shift) voltage generator are required.

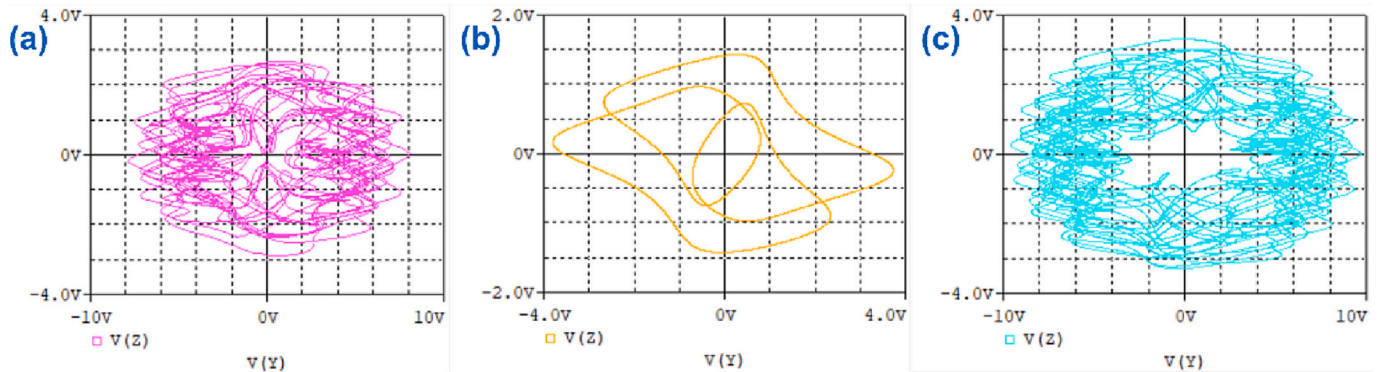


**Fig. 9.** The simulation results of the circuit from Fig. 8 in  $Y - Z$  plane. Projection of (a) chaotic attractor with  $z_0 = 0$ , (b) periodic attractor with  $z_0 = -0.3$ , and (c) torus attractor with  $z_0 = 2.2$ . The dynamics of an analog circuit agrees with the numerical results from Fig. 1.

The schematic of the designed circuit in the OrCAD simulation environment is provided in Fig. 8. Three integrators are used to implement the three state variables. Also, two inverters, a multiplier, a cosine function block, and a sinusoidal voltage generator are employed. The integrator and inverter circuits are designed based on operational amplifiers (OpAmps). The value of capacitors is  $C_1 = C_2 = C_3 = 100\mu F$ , and the resistors' values are set as  $R_1 = R_2 = R_3 = R_5 = 10k\Omega, R_4 = 100k\Omega, R_6 = R_7 = R_8 = R_9 = 1k\Omega$ . Moreover, the supply voltages of the OpAmps are  $V_p = 30V, V_n = -30V$ .

The cosine signal in the last line of System (5) is implemented by applying a  $\frac{\pi}{2}$  rad phase shift to the generated sine function. The frequency in the cosine signal is measured in  $\frac{rad}{s}$ , but the frequency measurement unit in OrCAD is Hz, so the frequency in Fig. 8 is set to 0.11 Hz according to

$$\omega = 2\pi f \rightarrow f = \frac{\omega}{2\pi} = \frac{0.7}{2\pi} \approx 0.11 Hz \tag{6}$$

The results of the simulation of the designed circuit from Fig. 8 are demonstrated in Fig. 9. To allow for a comparison with the previous numerical results, the attractors are projected on  $Y - Z$  plane with initial

conditions  $(x_0, y_0, z_0) = (0, 0, z_0)$  and (a)  $z_0 = 0$ , (b)  $z_0 = -0.3$ , and (c)  $z_0 = 2.2$ . The circuit's behavior matches the numerical results, recovering all chaotic, periodic, and torus attractors from Fig. 1.

### 5. Conclusion

In the present paper, we have provided the first example of a mega-extreme multistable chaotic system. The introduced three-dimensional non-autonomous system shows extreme and megastability under the variation of initial conditions corresponding to two different state variables. The megastability of our system has been corroborated by phase portrait projections demonstrating an infinite but countable number of coexisting attractors. The latter can conform to the same or different types of dynamics. To verify that the model exhibits genuine attractors, we have investigated the dissipative character of the system's dynamics by explicitly calculating the divergence, which turned out to be state-dependent. Nevertheless, the numerically determined average divergences for all the relevant regimes showed convergence to negative values, indicating that the system dynamics is indeed dissipative. Also, the connecting curves have been determined to better characterize the

system attractors.

Concerning the extreme multistability feature of the novel system, we have constructed the bifurcation diagram under the variation of the appropriate initial condition and have numerically determined the corresponding Lyapunov spectra and the Kaplan-Yorke dimension. The transitions between periodic and chaotic attractors observed in the bifurcation diagram have been corroborated by constructing the attraction basins in three planes of initial conditions. Finally, we have confirmed the validity of the numerical results by designing and simulating an analog circuit in the OrCAD environment. The circuit was designed using simply available components like OpAmps, resistors, capacitors, multipliers, and signal generators. We have shown that the circuit dynamics agrees well with the numerical results for the original system, demonstrating that the mega-extreme multistability feature is reproducible and flexible in applications. This is especially important given that there may be instances where the realization of solely extreme multistable or megastable systems may be difficult. We believe that discovering a new class of mega-extreme multistable systems will catalyze new research directions concerning the origin, design, and control of multistable nonlinear systems.

### Declaration of competing interest

The authors have no relevant financial or non-financial interests to disclose.

### Data availability

The authors admit that the data supporting the findings of this study are accessible through the paper.

### Acknowledgments

This work was supported by the Centre for Nonlinear Systems, Chennai Institute of Technology (CIT), India (Grant number [CIT/CNS/2023/RP/005]). I.F. acknowledges the funding provided by the Institute of Physics Belgrade through a grant by the Ministry of Science, Technological Development, and Innovations of the Republic of Serbia.

### References

- [1] Lorenz EN. Deterministic nonperiodic flow. *J Atmos Sci* 1963;20:130.
- [2] Strogatz SH. *Nonlinear dynamics and chaos: with applications to physics, biology, chemistry, and engineering*. Westview Press; 2014.
- [3] Degn H, Holden AV, Olsen LF. *Chaos in biological systems*. Springer Science & Business Media; 2013.
- [4] Lin H, Wang C, Cui L, Sun Y, Zhang X, Yao W. Hyperchaotic memristive ring neural network and application in medical image encryption. *Nonlinear Dyn* 2022;110:841.
- [5] Lin H, Wang C, Yu F, Sun J, Du S, Deng Z, et al. A review of chaotic systems based on Memristive Hopfield neural networks. *Mathematics* 2023;11:1369.
- [6] Chen G, Dong X. *From chaos to order: methodologies, perspectives and applications*. World Scientific; 1998.
- [7] Boccaletti S, Grebogi C, Lai Y-C, Mancini H, Maza D. The control of chaos: theory and applications. *Phys Rep* 2000;329:103.
- [8] Feudel U. Complex dynamics in multistable systems. *Int J Bifurcation Chaos* 2008;18:1607.
- [9] Pisarchik AN, Feudel U. Control of multistability. *Phys Rep* 2014;540:167.
- [10] Feudel U, Pisarchik AN, Showalter K. Multistability and tipping: from mathematics and physics to climate and brain—minireview and preface to the focus issue. *Chaos* 2018;28:033501.
- [11] Xu Q, Lin Y, Bao B, Chen M. Multiple attractors in a non-ideal active voltage-controlled Memristor based Chua's circuit. *Chaos, Solitons Fractals* 2016;83:186.
- [12] Xu Q, Cheng S, Ju Z, Chen M, Wu H. Asymmetric coexisting bifurcations and multistability in an asymmetric Memristive diode-bridge-based jerk circuit. *Chin J Phys* 2021;70:69.
- [13] Wang Z, Moroz I, Wei Z, Ren H. Dynamics at infinity and a Hopf bifurcation arising in a quadratic system with coexisting attractors. *Pramana* 2018;90:1.
- [14] Li C, Sprott J. Finding coexisting attractors using amplitude control. *Nonlinear Dyn* 2014;78:2059.
- [15] Li C, Wang X, Chen G. Diagnosing multistability by offset boosting. *Nonlinear Dyn* 2017;90:1335.
- [16] Wang Q, Yan S, Wang E, Ren Y, Sun X. A simple Hamiltonian conservative chaotic system with extreme multistability and offset-boosting. *Nonlinear Dyn* 2023;111:7819.
- [17] Li C, Lei T, Liu Z. Offset parameter cancellation produces countless coexisting attractors. *Chaos* 2022;32:121104.
- [18] Deng Z, Wang C, Lin H, Sun Y. A Memristive spiking neural network circuit with selective supervised attention algorithm. In: *IEEE transactions on computer-aided design of integrated circuits and systems*; 2022.
- [19] Liao M, Wang C, Sun Y, Lin H, Xu C. Memristor-based affective associative memory neural network circuit with emotional gradual processes. *Neural Comput & Applic* 2022;34:13667.
- [20] Lin H, Wang C, Tan Y. Hidden extreme multistability with hyperchaos and transient chaos in a Hopfield neural network affected by electromagnetic radiation. *Nonlinear Dyn* 2020;99:2369.
- [21] Zhang H, Sun K, He S. A fractional-order ship power system with extreme multistability. *Nonlinear Dyn* 2021;106:1027.
- [22] Hens C, Banerjee R, Feudel U, Dana S. How to obtain extreme multistability in coupled dynamical systems. *Phys Rev E* 2012;85:035202.
- [23] Ngonghala CN, Feudel U, Showalter K. Extreme multistability in a chemical model system. *Phys Rev E* 2011;83:056206.
- [24] Jin M, Sun K, Wang H. Hyperchaos, extreme multistability, and hidden attractors in the novel complex nonlinear system and its adaptive hybrid synchronization. *Nonlinear Dyn* 2022;110:3853.
- [25] Fossi JT, Deli V, Njitacke ZT, Mendimi JM, Kemwoue FF, Atangana J. Phase synchronization, extreme multistability and its control with selection of a desired pattern in hybrid coupled neurons via a Memristive synapse. *Nonlinear Dyn* 2022;109:925.
- [26] Zhang S, Zheng J, Wang X, Zeng Z. A novel no-equilibrium HR neuron model with hidden homogeneous extreme multistability. *Chaos, Solitons Fractals* 2021;145:110761.
- [27] Bao H, Gu Y, Xu Q, Zhang X, Bao B. Parallel bi-memristor hyperchaotic map with extreme multistability. *Chaos, Solitons Fractals* 2022;160:112273.
- [28] Zhang Y, Liu Z, Wu H, Chen S, Bao B. Two-memristor-based chaotic system and its extreme multistability reconstitution via dimensionality reduction analysis. *Chaos, Solitons Fractals* 2019;127:354.
- [29] Patel MS, Patel U, Sen A, Sethia GC, Hens C, Dana SK, et al. Experimental observation of extreme multistability in an electronic system of two coupled Rössler oscillators. *Phys Rev E* 2014;89:022918.
- [30] Hens C, Dana SK, Feudel U. Extreme multistability: attractor manipulation and robustness. *Chaos* 2015;25:053112.
- [31] Chen M, Luo X, Suo Y, Xu Q, Wu H. Hidden extreme multistability and synchronicity of memristor-coupled non-autonomous Memristive Fitzhugh–Nagumo models. *Nonlinear Dyn* 2023;111:7773.
- [32] Sprott JC, Jafari S, Khalaf AJM, Kapitaniak T. Megastability: coexistence of a countable infinity of nested attractors in a periodically-forced oscillator with spatially-periodic damping. *Eur Phys J Spec Top* 2017;226:1979.
- [33] Prakash P, Rajagopal K, Singh JP, Roy BK. Megastability, multistability in a periodically forced conservative and dissipative system with Signum nonlinearity. *Int J Bifurcation Chaos* 2018;28:1830030.
- [34] Jafari S, Rajagopal K, Hayat T, Alsaedi A, Pham V-T. Simplest megastable chaotic oscillator. *Int J Bifurcation Chaos* 2019;29:1950187.
- [35] Leutcho GD, Jafari S, Hamarash II, Kengne J, Njitacke ZT, Hussain I. A new Megastable nonlinear oscillator with infinite attractors. *Chaos, Solitons Fractals* 2020;134:109703.
- [36] Zhang K, Vijayakumar M, Jamal SS, Natiq H, Rajagopal K, Jafari S, et al. A novel Megastable oscillator with a strange structure of coexisting attractors: design, analysis, and FPGA implementation. *Complexity* 2021;2021:2594965.
- [37] Li R, Dong E, Tong J, Du S. A new autonomous Memristive megastable oscillator and its Hamiltonian-energy-dependent Megastability. *Chaos* 2022;32:013127.
- [38] Gilmore R, Ginoux J-M, Jones T, Letellier C, Freitas U. Connecting curves for dynamical systems. *J Phys A Math Theor* 2010;43:255101.
- [39] López-Rentería JA, Aguirre-Hernández B, González F Verdúzco. On Hurwitz and Schur connecting-curves and dense trajectories. In: *Advances in Mathematical and Computational Methods: Addressing Modern Challenges of Science, Technology, and Society*. 1368; 2011. p. 271.
- [40] Byrne G, Gilmore R, Cebral J. Connecting curves in higher dimensions. *J Phys A Math Theor* 2014;47:215101.
- [41] Guan X, Xie Y. Connecting curve: a new tool for locating hidden attractors. *Chaos* 2021;31:113143.
- [42] Frederickson P, Kaplan JL, Yorke ED, Yorke JA. The Liapunov dimension of strange attractors. *J Differ Equ* 1983;49:185.
- [43] Kaplan JL, Mallet-Paret J, Yorke JA. The Lyapunov dimension of a nowhere differentiable attracting torus. *Ergodic Theory Dynam Syst* 1984;4:261.